Fluctuation spectroscopy of step edges on Pt(111) and Pd(111)

M. Ondrejcek,[1,2,*] W. Swiech,[2] M. Rajappan,[1,2] and C. P. Flynn[1,2]
[1]*Physics Department, University of Illinois at Urbana-Champaign, Urbana, Illinois 61801, USA*
[2]*Materials Research Laboratory, University of Illinois at Urbana-Champaign, Urbana, Illinois 61801, USA*
(Received 10 November 2004; revised manuscript received 22 March 2005; published 8 August 2005)

By step fluctuation spectroscopy, using low-energy electron microscopy (LEEM), we investigate step energies and relaxation on clean Pt(111) and Pd(111) surfaces at temperatures above half the melting temperature T_m. Some effort has been expended to develop accurate procedures for analyzing fluctuations observed as video recordings. The average step stiffnesses are about 210 meV/nm and 265 meV/nm for Pt and Pd, weakly temperature dependent, and in each case fairly isotropic with mainly a sixfold angular variation. Consequently, the step free energies are highly isotropic. At the lower temperatures, the relaxation rates of fluctuations with wave vector, q, vary as q^3. This is the unambiguous signature of step relaxation by surface diffusion over the terraces. It affords accurate determinations of the surface mass diffusion coefficients $D_s=5(\times 2^{\pm 1})\times 10^{-4}\exp(-1.2\pm 0.1\ \mathrm{eV}/k_BT)\ \mathrm{cm}^2/\mathrm{s}$ for Pt(111) and $D_s=3(\times 2.5^{\pm 1})\times 10^{-3}\exp(-1.1_5\pm 0.1_5\ \mathrm{eV}/k_BT)\ \mathrm{cm}^2/\mathrm{s}$ for Pd(111). At more elevated temperatures the measured rates vary approximately as q^2 in both cases. This corresponds to the surface process being short-circuited by a faster flow of bulk vacancies. Known bulk diffusion coefficients for Pt and Pd are consistent with this interpretation. An effective procedure is developed to separate bulk and surface contributions. There is the appearance of universality in the fluctuation processes, which approximates as an homologous dependence on T/T_m. It is observed for Pt(111) at 1400 K and above that neighboring steps react to form multisteps that retain capillary characteristics. The stiffnesses of multisteps formed from up to five associated steps have been determined by fluctuation spectroscopy and are employed to discuss the energetics of multistep formation. Clear evidence is found that the multistep free energy contains important contributions from internal degrees of freedom. The kinetics of multistep fluctuations are explained by the same diffusion coefficient D_s determined from single steps.

DOI: 10.1103/PhysRevB.72.085422 PACS number(s): 68.35.Fx, 68.37.Nq, 66.30.−h

I. INTRODUCTION

This paper reports kinetic and energetic properties of clean Pt(111) and Pd(111) surfaces in a range of temperatures that lies above half the melting temperature T_m. The main kinetic information appears as values for the surface mass diffusion coefficient D_s of the surface in thermal equilibrium. D_s measures the rate at which tracers at equilibrium on the surface progress distance R according to $R^2=4D_st$, with t the elapsed time. In the simplest case, when a single-defect mechanism is dominant, D_s is the product of the (temperature-dependent) hopping diffusion coefficient D of adatoms,[1,2] presumed to be the dominant thermal defects, and their (temperature-dependent) fractional occupancy of surface sites. Each factor is thermally activated, so D_s obeys an Arrhenius relationship with an activation energy equal to the sum of formation and hopping parts. Hopping rates of adatoms have been widely explored.[3] However, neither the thermal concentrations nor the mass diffusion is easy to measure, so that the typical behavior of D_s on clean metal surfaces still remains largely to be established. It is important here that D_s also determines the surface flux that flows in response to a gradient of chemical potential such as that created by a curved step.

The energetic characteristic of a curved step that drives local mass flow is the Gibbs-Thompson potential $\mu=\tilde{\beta}\chi$ with χ the step curvature and $\tilde{\beta}$ its stiffness. The stiffness is related to the step free energy β per unit length by[4]

$$\tilde{\beta}=\beta+\partial^2\beta/\partial\theta^2, \tag{1}$$

in which θ is the azimuthal angle of the step. Here we define θ by the downhill normal to the step, measured relative to some crystallographic axis. The profile of a step fluctuates in time as thermal defects are transferred between the step and the adjacent terraces. It turns out that the kinetics of the profiles are determined by D_s and $\tilde{\beta}$. Thus a study of step fluctuations can be used to measure both the step free energy and surface diffusion.[5–7]

We are engaged in an extended program that employs the spectroscopy of step fluctuations, observed by low-energy electron microscopy (LEEM), to explore diffusion and step energetics on the close-packed surfaces of refractory and noble metals. For these materials, vacuum compatibility makes results reasonably reproducible. LEEM yields video output of micron-sized areas with ~10 nm resolution at 30 frames per second, characteristics that are well suited to the capillary fluctuations (see below) of steps on metal surfaces at temperatures $\sim T_m/2$. Our recent effort have concerned Mo(011) (Ref. 8) and Au(111) (Ref. 9). The present research reports detailed results for two similar and almost ideal close-packed surfaces Pt(111) and Pd(111). Brief reports of results for Pt steps[7] and multisteps,[10] using a preliminary procedure for analysis of video records, point in addition to important features of energetics and kinetics that behave systematically among alternative surfaces.[11] Examples are the observation that diffusion is approximately universal among

surfaces, when viewed as a homologous function of T/T_m, and that step stiffnesses in this range are unexpectedly small and temperature insensitive. Optimized procedures for deriving step and terrace properties from video tape are lacking from the pioneering efforts that used LEEM (Ref. 6) and reflection electron microscopy (REM) (Ref. 5) for these purposes, so a significant part of our subsequent research has been to develop reliable new procedures, described below. The application of these improved methods to Pt cause the deduced values of stiffness and D_s to change by factors up to 50% in a nonsystematic manner, so these are matters of some interest for future research. The purpose of the present paper is to report, first, the required improvements of methods for data analysis, second the resulting stiffness and kinetic properties these procedures yield for the similar surfaces of Pt(111) and Pd(111), and finally to assess the light these results shed on the possibility raised earlier that surface properties behave systematically among different metal surfaces.

The step fluctuation spectroscopy employed in this research originates in ideas of capillarity developed for two-dimensional (2D) objects[12] and first applied to the analogous 1D energetics of step edges later by Nozieres.[13] In a Fourier decomposition,

$$y(x,t) = \Sigma_q y_q(t) \exp iqx, \tag{2}$$

for a step of length L, and $q = 2\pi q/L$, q integral, the added free energy is of second order,

$$U\{y_q\} = \frac{1}{2}\Sigma_q \tilde{\beta} q^2 \langle |y_q|^2 \rangle, \tag{3}$$

and accordingly the amplitudes have Gaussian distributions with

$$\langle |y_q|^2 \rangle = \frac{k_B T}{\tilde{\beta} L q^2}. \tag{4}$$

In effect, the q^{-1} variation of the mean amplitude with q is a definition of capillarity and the attendant dependence of energy on displacement. This exact result also affords a means to obtain $\tilde{\beta}$ from direct observation of steps, as pioneered using LEEM (Ref. 6) and REM (Ref. 5) for Si(001). It needs to be mentioned that while Eq. (2), as employed, takes the step to be periodic in L, this is not true in actual images, and there are practical repercussions in the analysis that are not under complete control. At the 10 nm resolution offered by LEEM, atomic details of step profiles are entirely suppressed, and the pertinent step fluctuations with wavelengths $\sim 10^2 - 10^3$ nm do have a smooth appearance, just as conceived in the capillary theory that leads to Eqs. (2)–(4). One can show also that the time correlation of the Fourier amplitudes obeys

$$\langle y_q(t) y_q^*(t') \rangle = \langle |y_q(t)|^2 \rangle \exp - |t - t'|/\tau_q, \tag{5}$$

with τ_q the relaxation time for Fourier mode q.[14,15]

It is important for this research that the decay kinetics can be discussed for very general models of the diffusion process, without added statistical assumptions, and for general reaction conditions of arbitrary transport mechanisms at the step edges.[15] A variation of $\tau_q^{-1} \sim q^3$ provides a specific signature that such reactions do *not* dominate (this will generally be the case for metals at high temperatures) and that mass diffusion over the terraces, by any operative microscopic mechanism, is the pathway by which relaxation takes place.[6,14,15] Under these conditions, the unambiguous prediction is that

$$\tau_q^{-1} = 2A\tilde{\beta} D_s a q^3 / k_B T. \tag{6}$$

Here, A is the surface area per atom and a the interlayer spacing. Alternative mechanisms have different signatures.[4,16] In particular, mass diffusion through the bulk, regardless of mechanism, causes relaxation approximated by[15,17]

$$\tau_q^{-1} = \pi A \tilde{\beta} D_b q^2 / a k_B T, \tag{7}$$

with a D_b the coefficient for *bulk* mass diffusion.

The above equations follow generally from the Nernst Einstein equation for flow and the capillary nature of the fluctuating object.[15] Accordingly, they are expected to find application for other capillary objects in addition to single steps. An example is the multistep, recently defined as step complexes that retain capillary characteristics,[10] formed by the association of almost-parallel steps. Facets also form in this way and retain capillary behavior such as fluctuations (e.g., on Nb films[18]) but may be distinguished by the appearance of locking to primitive crystallographic azimuths. Step reactions are observed on clean surfaces,[9,19,20] on adsorbate-covered surfaces,[21,22] and step bunches form through growth instabilities.[23] Configurations of one to four steps have been observed on Si(113) after quenching.[24] In a preliminary report we described a variety of multisteps with different heights that form on Pt(111) at temperatures above about 1400 K.[10] Their energetics and kinetics are reported and discussed more precisely in the present paper.

The step free energy and the surface energy of terraces determine the energy per unit of a multiterrace surface as the surface energy together with the step energies (and the step-step interactions).[25,26] Values of the step stiffness as a function of orientation for isolated steps thus provide a path to the basic energetics of surfaces. Even for clean, vacuum-compatible metal surfaces, the available information presents an uncertainty of almost an order of magnitude in the typical value of $\tilde{\beta}$ for clean metals.[8,27,28] In the case of Pt(111), relevant here, measurements using scanning tunneling microscopy (STM) below 500 K have been interpreted in terms of stiffnesses $\sim 3-4$ eV/nm,[16,28] whereas a preliminary account of the present research gave a value ~ 0.2 eV/nm above 900 K.[7] Differences of this magnitude among observed properties reflect the primitive character of present knowledge, which theory has not been able to resolve. The stiffness could possibly decrease abruptly between these temperatures. It has long been anticipated that metal surfaces may exhibit a step roughening transition above which the step free energy is greatly reduced in this way.[25,29] Arguments for this transition stand mainly on entropic factors due to the proliferation of kinks on the step profile. Experiments described below suggest that the typical behavior is *not* in accordance with these expectations.

Each of the (face-centered-cubic) refractory metals Pt and Pd, chosen for this study, is well suited by low reactivity to the UHV conditions required for experiments on clean surfaces, and their (111) surfaces have been the subject of numerous prior investigations that we now summarize. The various techniques employed include low-energy electron diffraction methods,[30–32] photoemission spectroscopy,[33–35] x-ray,[36,37] ion[38,39] and He atom scattering,[40,41] scanning tunneling microscopy,[42–45] low-energy electron microscopy,[46] reflection electron microscopy,[47] and ion erosion.[48] It is pertinent that the LEEM studies[46] of islands on Pt (111) above 1100 K observe effects of bulk vacancies being created at the free surface. Clean Pt(111) and clean Pd(111) are both known to lack reconstruction at room temperature and low pressure, but Pt(111) reconstructs reversibly above 1330 K (Refs. 30, 31, 36, and 37) and also reconstructs under supersaturated Pt vapor at 400–700 K (Refs. 42 and 43). The Pt(111) reconstruction increases the surface density of atoms by 4% to create alternating domains of ideal fcc stacking and faulted hcp stacking, separated by disordered arrangements of misfit surface dislocations referred to as double stripes. The double stripes on Pt(111), symmetry $3m$, lie along three equivalent orientations and leave the surface under isotropic compression. They are observed for both the high- and low-temperature reconstructions. At low temperatures the stripes form a hexagonal honeycomb structure with cells varying from 10 to 30 nm. An increase of chemical potential drives the honeycomb pattern towards an appearance of wavy triangles and star structures.

In what follows, Sec. II outlines the main features of equipment, sample handling, and data acquisition and provides details of the data analysis procedures developed to obtain quantitatively reliable stiffnesses and diffusion coefficient. The main results of our investigations of single steps and multisteps on Pt(111) and Pd(111) are then presented in Sec. III. Section IV interprets the results and places the cases of Pt and Pd in the broader context of surface properties.

II. EXPERIMENT

The present study of Pt(111) and Pd(111) follows work on Mo(001), Nb(011), and Au(111) that employs the same equipment and similar methods. For this reason, the present account of equipment and procedures is concise, with reference to more complete description elsewhere when possible.

A LEEM built at IBM, with operating characteristics described by Tromp and Reuter,[49] was employed in this research. Its upper chamber has been extensively rebuilt in-house to conveniently accommodate various sample manipulations including sample introduction, processing, and growth. Techniques relevant to the present work include *in situ* Ar^+-ion sputtering and Auger analysis. The LEEM has a base pressure maintained in the 10^{-11} torr range. It is capable of operating at sample temperatures up to 1700 K, using electron beam heating directed to the rear of the sample. Temperatures were measured to ±15 K using a disappearing filament pyrometer above 1000 K and an infrared optical pyrometer over the entire range of the present experiments.

Platinum and palladium fcc crystals were purchased from the Surface Preparation Laboratory in the form of disks 1 mm thick and 9 mm in diameter, and oriented (111) to within ~0.1°. Care was taken to ensure that the sample face was fully cleaned before measurements were undertaken. Prior to introduction into the LEEM they were cleaned in an auxiliary vacuum chamber by many cycles of Ar^+-ion sputtering at room temperature followed by anneals at 1300 K for Pt(111) and 1100 K for Pd(111), with occasional O_2 exposure. A sharp LEED pattern with no additional spots and a low secondary background were finally achieved in each case before the crystal was placed in the LEEM. Once there, a similar cycling was renewed briefly to restore the pristine surface. Auger analysis revealed no foreign species, with $<1\%$ sensitivity.

Large areas of the Pt and Pd surfaces were relatively perfect, with steps reasonably parallel and well spaced, consistent with the average surface miscut. For Pt it proved difficult to find regions with sufficiently varied step orientations to afford an opportunity to explore angle dependent factors. Typical views of the cleaned surfaces at elevated temperatures are given for Pt and Pd in Figs. 1(a) and 1(b), respectively. It is apparent that the two surfaces are almost ideal for step fluctuation studies. In this research, 65 lines were studied on Pt(111) at 11 temperatures, comprising 53 single steps and 12 multisteps. All 60 steps studied for Pd were single steps.

Our procedures for step profile analysis continue to be refined, but remain in part as described in an earlier report.[7,8] Digitized images were rotated to a convenient orientation, and the step profile was identified by fitting a Gaussian to the line intensity profile, thereby locating a line center for each row to a fraction of a pixel. The bilinear rotation had no negative impact on image quality. An example of Pt steps, marked along their lengths by such fitted centers, is given in Fig. 2(a), with intensity profile below. Sequences of 1–2 min of frames at video rates ($f=30\ s^{-1}$), making more than 10^3 frames per run, were processed and then fast Fourier transformed (FFT) to obtain the $y_q(t)$ as a time sequence. From these, $\langle|y_q(t)|^2\rangle$ and $\langle y_q(t)y_q^*(t')\rangle$ could be obtained by straightforward methods. Any residual inclination of the average line relative to the zero axis causes the Fourier components of a triangle to be added to those of the fluctuations. To eliminate errors of the average slope we employed a "triangle subtraction."

Figure 2(b) shows an example the variation with q of $\langle|y_q(t)|^2\rangle$ for Pd at 1090 K. The open points represent raw data, and the solid points are the same results when the spatial and temporal bandwidths of the LEEM are deconvolved from the output, as detailed elsewhere.[8] There is excellent agreement with the dependence on q^{-2} predicted by capillary theory, through Eq. (4). Equally satisfactory results were found in almost all other cases. The noise power in the Fourier amplitudes is evidently low enough, since the data yield consistent experimental values of $\langle|y_q(t)|^2\rangle$, for q as large as 22 for Pt at low temperatures. At high temperatures, results were confined to a smaller range of q values, where relaxation rates approached the limiting video rate. The independent results for so many Fourier components provide an excellent opportunity to explore step kinetics, as illustrated inset in Fig. 2(b). There, values of $\tilde{\beta}$ derived for different q,

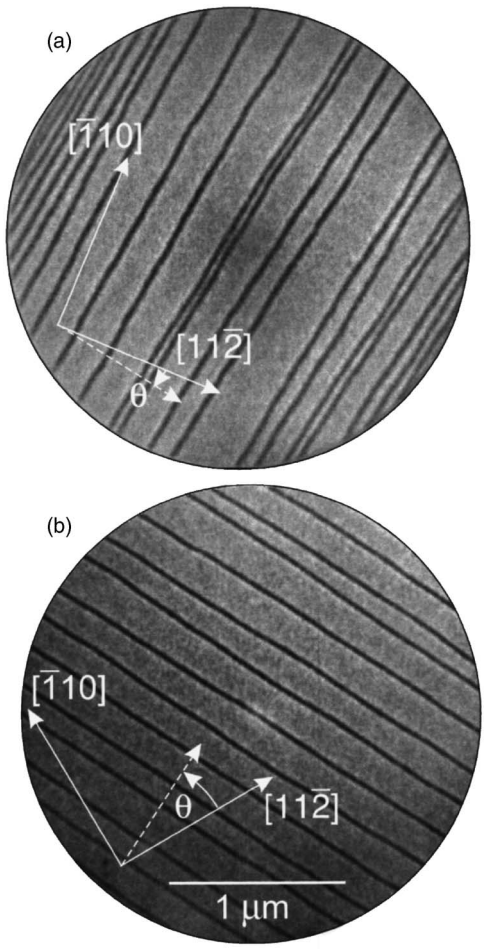

FIG. 1. (a) LEEM micrographs showing Pt(111) surface features at 1375 K and an impact energy $E=5$ eV. Almost ideal straight single step edges are visible. The step angles studied here have $-14° < \theta < -4°$. (b) The Pd(111) surface at 1235 K taken with $E=20$ eV, $\theta=26°$. The step angles studied have $-6° < \theta < 65°$. For each image, the broken arrow indicates the average step orientation (normal to the length) relative to the close- packed direction. The orientation is based on a LEED image not shown. The field of view is 2.6 μm.

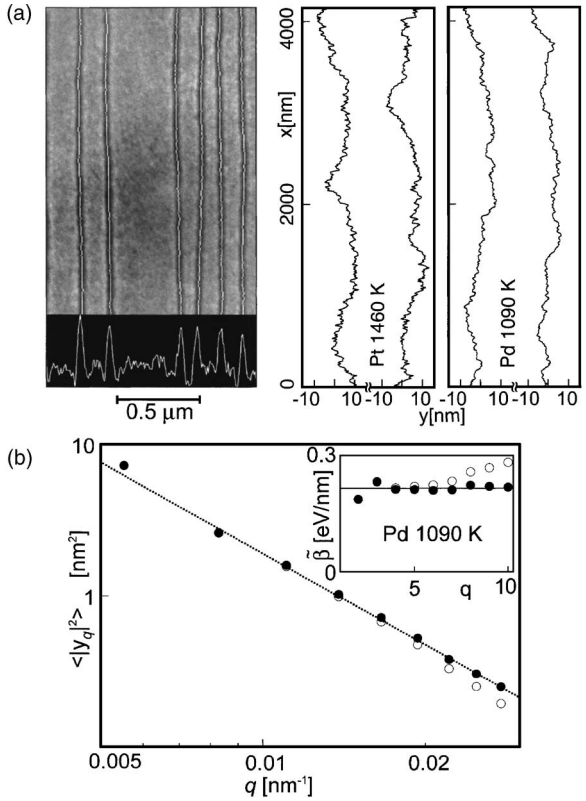

FIG. 2. (a) The left panel shows steps marked by fitting Gaussians to the intensity profiles, for Pt(111) at 1330 K, with $E=18$ eV. Right panel shows step profiles at a 2-s interval at 1460 K for Pt(111) and at 1090 K for Pd(111). (b) Squared Fourier amplitudes shown as a function of q for a single Pd step at 1090 K. Open circles represent raw data, and solid points are data corrected for constant pixel noise, spatial, and temporal resolutions. A straight line fit shows the q^{-2} dependence of amplitudes. Inset shows the variations of stiffness with q calculated using Eq. (4). 1 frame $(1f)=1/30$ s, q [nm^{-1}]$=2\pi$q$/L$, q$=1,2,\ldots$, integral, and with $L \sim 2.2$ μm.

directly from the respective amplitudes, exhibit a satisfactory scatter about a common mean.

There nevertheless occurs some spurious noise in the Fourier amplitudes, apparently associated with the cutoff of the step at each end of the arbitrary length L, typically ~ 2.2 μm. In the manipulation of Fourier data such end effects are often handled using a "window" function[50] designed to reduce end effects. Of these, the best known "Hanning" window multiplies the profile prior to its FFT by $[1-\cos(2\pi y/L)]/2$ to deemphasize displacements at the two ends. Because any such window distorts the resulting amplitudes as functions of q, window procedures cannot properly be employed to obtain $\langle|y_q(t)|^2\rangle$. In the case of time correlations, however, we found that the Hanning window gave a considerable reduction of experimental noise, as evidenced by the scatter of the data, without systematic modification of the deduced relaxation times, within the uncertainties, although individual results are changed. This is illustrated by an example shown in Fig. 3 and described in what follows.

Figure 3(a) shows the normalized time correlation $\langle y_q(t)y_q^*(t')\rangle/\langle y_q(t)y_q^*(t)\rangle$ for Pd at 1090 K, evaluated for several Fourier components q, for both the triangle subtraction [see Fig. 3(a)] and Hanning [see Fig. 3(b)] procedures. An initial point of importance in (a) is that the normalized time correlation is expected, by definition, to decay from 1 at $t'=t$ to 0 at $t'-t\to\infty$. Instead, the observed correlations often decay to a substantial and nonzero value. This happens mainly because the line is bent or rotated by local strains or other fields on the surface, so that the final relaxed shape has nonzero Fourier components. Given this interpretation, the correct time correlation requires that the $t\to\infty$ value be subtracted for all earlier times. In this connection it is noteworthy that the Hanning window often reduces the erroneous correlations at long times, presumably because any average curvature causes its largest displacements at the ends. It is an important matter that this correction applies additionally to the $t=0$ value $\langle|y_q(t)|^2\rangle$. In our use of the triangle subtraction to determine stiffness, the deduced values of the step stiff-

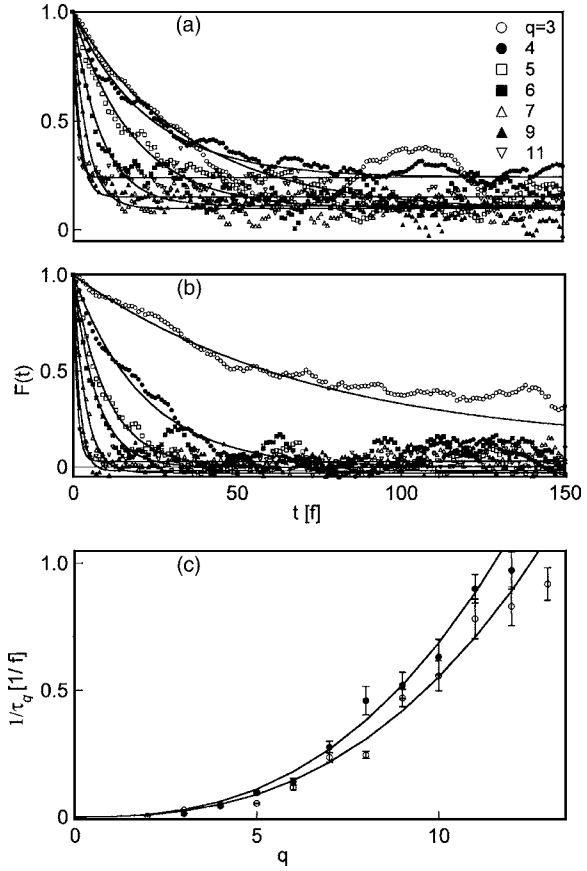

FIG. 3. Relaxation times obtained from fits to time correlations $F(t)$ for Pd(111) at 1090 K. (a) With the "triangle" subtraction, FFT's calculated from profiles with average slope subtracted often exhibit an offset as $t' \to \infty$ that must be subtracted in a calculation of the stiffness. Thus corrected $\tilde{\beta}=0.27$ eV/nm for the data set of Fig. 2. (b) With the Hanning window function applied to the profiles to suppress end effects, the relaxation times do not show big changes from (a) but offsets are greatly reduced. (c) Comparison of the "triangle" subtraction (open circles) and the Hanning analysis (solid circles). The power dependence q^{α} fits with $\alpha=2.64\pm0.19$ and $\alpha=2.62\pm0.19$ in the two cases, and the two methods yield relaxation times differing here by 25%.

nesses are increased by the elimination of the spurious correlations that arise from static step structure, thus identified.

Returning now to the use of window functions, Fig. 3(c) shows how fitted values of τ_q^{-1} obtained from the data in Figs. 3(a) and 3(b) using triangle and Hanning methods, respectively, each vary with q. Several matters are clarified by this graph. First, the two methods do yield similar exponents, so that the power-law dependence is fitted as $q^{2.62}$ and $q^{2.64}$ in the two cases. Second, the scatter of points is noticeably less for the Hanning procedure. Third, the exponents are quite close to the value 3 predicted for relaxation driven by surface diffusion [cf. Eq. (5)]. This is central to the identification of surface mass diffusion coefficients in Sec. III. Finally, the absolute magnitude of the relaxation time is modified by ~25%, and the changes enter directly into deduced diffusion coefficients.

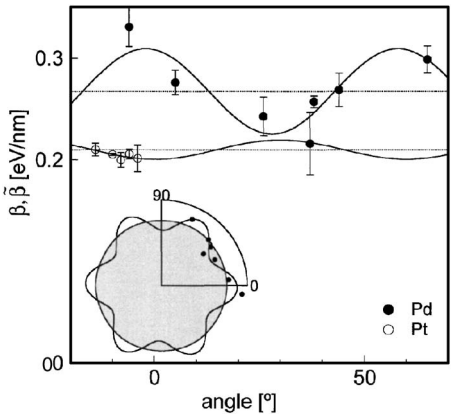

FIG. 4. Mean orientation dependence of the stiffnesses. Experimental data for Pd (solid circles) and Pt (open circles) were fitted to the constant and cos 6θ terms of a Fourier series. The best mean-square fit for Pd is obtained for $-2°$ azimuth. The isotropic part is $\tilde{\beta}=0.27$ eV/nm for Pd(111) at 1190 K and $\tilde{\beta}=0.21$ eV/nm for Pt(111) at all temperatures given a weak T dependence of $\tilde{\beta}$ (see Fig. 5). The Pt surface was smoother than Pd so steps occupied a limited range of angles. Inset shows polar plot of the almost isotropic step free energy (gray shaded area) of Pd(111) obtained from the stiffness.

III. RESULTS AND ANALYSIS

The results presented here are organized for convenience into three areas respectively concerning step stiffness, diffusion driven kinetics, and multistep behavior.

A. Step stiffness

It is shown above that the step stiffness follow directly from $\langle |y_q(t)|^2 \rangle$, subject to possible corrections from any remaining correlation at $t \to \infty$. Because the measured stiffness enters as a significant factor into the analysis of kinetics, it is most convenient to deal with the stiffnesses first.

From the measured squared amplitudes, for steps of different orientation at a selected temperature, we have determined the dependence of $\tilde{\beta}(\theta)$ on θ for Pd and, to a lesser degree, for Pt. The final values are shown in Fig. 4. There, the results for Pd at 1190 K, shown as solid circles, cover an angular range of 70°. This range is sufficient to define the angle dependence almost completely for the given $(3m)$ surface symmetry. The observed values do not depart far from isotropy, and the deviations seem consistent with mainly a sixfold departure alone. The solid line through the angle-dependent data represents the fit

$$\tilde{\beta}(\theta) = 270 \pm 15 + (40 \pm 10)\cos 6\theta \text{ meV/nm}. \quad (8)$$

The best fit gives the angular reference at 2°, close to the expected symmetry of about $[11\bar{2}]$.

For the case of Pt our results are less complete because the surface was macroscopically smoother and so offered less opportunity to study steps over a wide range of angles. Steps were nevertheless explored over a range ~14° of orientations, with results presented in Fig. 4 as open circles.

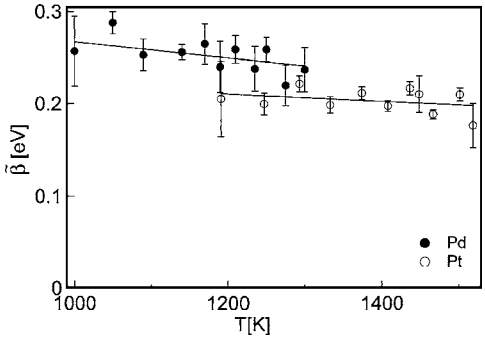

FIG. 5. Average stiffnesses along the prevalent miscut for Pt(111) (open circles) and Pd(111) (solid circles) showing their weak temperature dependence.

The available range is much too small to afford a definitive measurement of $\tilde{\beta}(\theta)$, and further analysis depends on an assumed functional form. In an earlier effort we employed a threefold deviation from isotropy, in keeping with the basic symmetry of the terrace. However, ancillary observations of small islands at these temperatures have since suggested that the threefold component of the free energy is small, leaving an observed sixfold island anisotropy, as in Eq. (8) for Pd. A fit of this assumed form to all the data yields the result

$$\tilde{\beta}(\theta) = 210 \pm 15 - (10 \pm 5)\cos 6\theta \text{ meV/nm} \qquad (9)$$

for Pt. Evidently the step stiffness for Pt is more isotropic than that for Pd at these temperatures. Note that the step free energy follows from a Fourier transform of Eq. (9) with the same isotropic term and the sixfold ($n=6$) anisotropy a factor $-(n^2-1)=-35$ smaller that that of the stiffness, as indicated inset in Fig. 4 for Pd. Our measurements thus show that the step free energy is remarkably isotropic for these surfaces. This contrasts with a large anisotropy observed under similar conditions for Au(111).[9] At the present time there exists no explanation for the factors that enter into anisotropy of step stiffness for individual metals.

Of considerable added interest is the temperature dependence of the step stiffness. For Pt and Pd the step stiffnesses are shown as functions of temperature in Fig. 5. These results were obtained by assuming, for lines close to the prevalent miscut, that $\tilde{\beta}$ could be factored into two terms: one angle dependent and the other temperature dependent. For Pt and Pd the mean step stiffnesses decrease only weakly with temperature. The Pd data set reported here are distinct from a set reported earlier, and it is reassuring that the two agree reasonably well.[27]

B. Step kinetics and diffusion

In this section we present mode relaxation times determined by step fluctuation spectroscopy and interpret them in terms of microscopic diffusion mechanisms. As described in Sec. II, relaxation times determined with use of the Hanning window function provide the most precise measure of the rates, and for this reason the procedure is employed for all the results reported in this section.

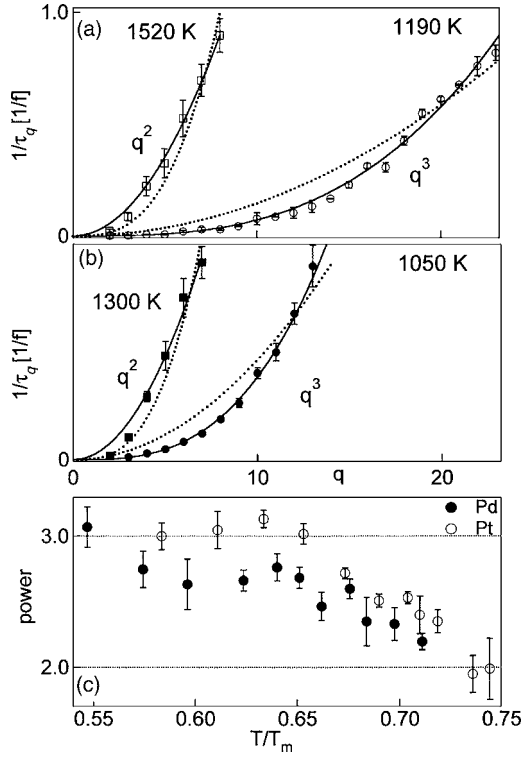

FIG. 6. (a) The dependence of the measured relaxation times on wave vector q for Pt(111) at 1190 K (open circles) and at 1520 K (open squares). Rates τ_q^{-1} vary closely as q^3 at low temperature as expected for relaxation limited by terrace diffusion and as q^2 at high temperature (solid lines). The dashed lines show reversed q^2 rate and q^3 for comparison. (b) Similar graphs for Pd(111) at 1050 K (solid circles) and 1300 K (solid squares). (c) The variation of averaged power law α for all lines as a function of T/T_m. 1 frame $(1f)=1/30$ s, q [nm^{-1}]$=2\pi$q$/L$, q$=1,2,\ldots$, integral, $L\sim 2.2$ μm.

A valuable feature of the present research is the ability to track the microscopic mechanism to which the observed relaxation may be attributed. In this connection, Fig. 6(a) shows for Pt and Fig. 6(b) for Pd the dependence of relaxation rate on wave vector index q at selected temperatures. The power laws of fits to such data show a change of exponent from roughly 3 to 2, from low to high temperature, in both data sets, as the selected examples indicate. From the complete results in Fig. 6(c) the transition centers on $T/T_m \sim 0.67$ for Pt(111) and ~ 0.65 for Pd(111).

The variation as q^3 at low temperatures ($\sim T_m/2$) is central to the interpretation of the data. Of comparable interest is the observation that the behavior at higher temperatures approaches a different limit of $\sim q^2$. As far as is currently known, the q^3 dependence is the unambiguous signature of diffusion to steps over the neighboring terraces,[4,14,15] as reviewed in Sec. I. In this process, surface defects pass from regions of high chemical potential on a step to regions of low chemical potential by flow loops that pass over the terraces. Therefore the relaxation times determined at low T by Fig. 6 may be attributed with some confidence to surface diffusion. Absolute values of D_s may then be derived by use of Eq. (6). In contrast, several mechanisms can possibly create the q^2 dependence of relaxation that is clearly observed for both

metals at higher T. These include two that can be ruled out. Of these the first is relaxation depressed by slow defect reactions at the step, which is compatible neither with the observed speed of relaxation nor with the likely size of Ehrlich-Schwoebel barrier[51,52] in these metals at high temperatures. A second is that alternative sinks for defect flow adjacent to the steps, including other steps, modify the kinetics,[4,16] which is not consistent with the observed clean, wide terraces. A process of greater interest here is the effect of bulk vacancies in short-circuiting the surface process by alternative flow loops that pass through the bulk and provide a more effective mechanism at high temperature. For several decades, quantitative measurements have been available for bulk diffusion at high temperature in a wide variety of metals, including Pt and Pd.[53] As a result it is possible to predict beforehand, with reasonable accuracy, the contribution that bulk diffusion makes to step relaxation on both Pt and Pd. This turns out to be the dominant mechanism for step relaxation at high temperatures.

Ondrejcek *et al.*[7] treat data approximately by assuming that surface and bulk processes simply add. In this way they obtain the equation

$$\frac{k_B T\Omega}{\pi\tau_q \beta q^2 A^2} = \mathrm{D}_b + (2qa/\pi)\mathrm{D}_s. \tag{10}$$

Figure 7(a) for Pt(111) shows for various temperatures the quantity on the left, plotted as a function of q for the best data, which include only $\mathrm{q} > 2$ and $\tau_q^{-1} < 25\ \mathrm{s}^{-1}$ ($30\ \mathrm{s}^{-1}$ is the frame rate). The data for the lowest four temperatures are linear in q with at most small intercepts at $\mathrm{q}=0$ [see also the inset in Fig. 7(a)]; from Eq. (10), this identifies the process with surface diffusion. From the slopes so determined, $\mathrm{D}_s(T)$ is shown against T_m/T in Fig. 8(a). The surface fraction for the higher temperatures in Fig. 8(a) is small and poorly determined. The resulting intercepts in Fig. 7(a) are shown in Fig. 8(b) as values of the bulk diffusion D_b.

The line passing near the points in Fig. 8(b) compares the resulting values with the values determined decades ago by radio tracer methods. The solid line through the data represents the tracer result $\mathrm{D}_b = 0.57 \exp(-2.85\ \mathrm{eV}/k_B T)\ \mathrm{cm}^2/\mathrm{s}$ determined for the particular temperature range.[54] We remark that there are no adjustable parameters whatever in this comparison of tracer results with the present data. Thus the radio tracer results are seen to afford a remarkably effective prediction for the observed step fluctuation spectra in the bulk-dominated regime. The coarse dotted line below the data points indicates other Pt diffusion measured[55,56] by radio tracer methods, but taken at higher temperatures and extrapolated into the present temperature range. While curvature of diffusion plots is documented[53,57] and may be the origin of the visible difference between the different sets of tracer results, it must be recognized also that the uncertainties of activation energies, as determined by tracer measurements, also can account for differences of this magnitude.

A similar analysis of Pd results is shown in Fig. 7(b). There is a smaller proportion of bulk diffusion in the range studied, so that the surface diffusion can be followed further. The resulting plot of D_s is presented in Fig. 8(a) as solid

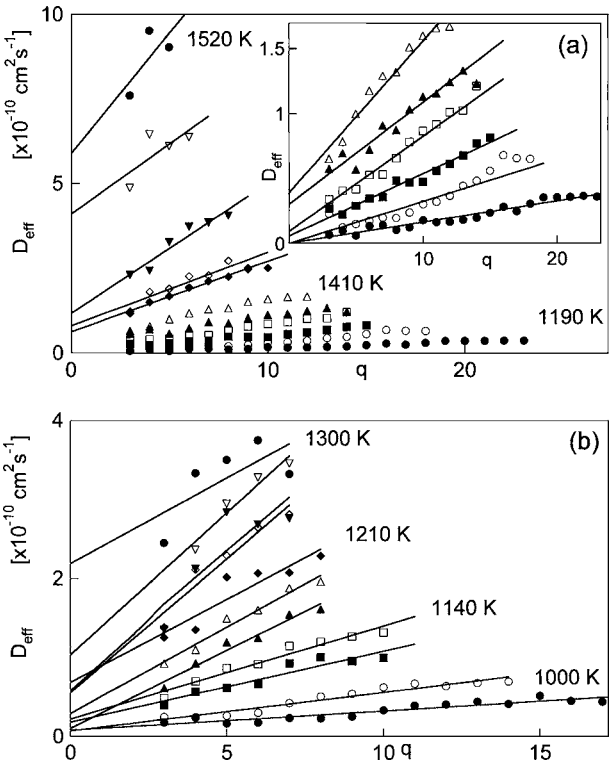

FIG. 7. Effective diffusion coefficients plotted as a function of wave number q from Eq. (10) for (a) Pt(111) and (b) Pd(111). At any given T, the slope fixes the D_s and the intercept gives D_b. For actual temperatures see Fig. 6(c). Inset of (a) shows fits for Pt(111) at low T, giving $\mathrm{D}_s = 5\times10^{-4} \exp(-1.2\ \mathrm{eV}/k_B T)\ \mathrm{cm}^2\ \mathrm{s}^{-1}$ and $\mathrm{D}_b \sim 0.8 \exp(-2.85\ \mathrm{eV}/k_B T)\ \mathrm{cm}^2\ \mathrm{s}^{-1}$ (the latter is not accurately determined). The fit for Pd(111), inset in (b), yields $\mathrm{D}_s = 3\times10^{-3} \exp(-1.1_5\ \mathrm{eV}/k_B T)\ \mathrm{cm}^2\ \mathrm{s}^{-1}$.

circles. Using the same procedure as for Pt it is possible to identify some contribution of bulk diffusion at the higher temperatures, although the quantitative values are not sufficiently certain to warrant detailed analysis. A fine dotted line in Fig. 8(b) represents the tracer results extrapolated from high temperature.[58] The values inferred here are substantially larger, and it is not known whether this arises from curvature or from the combined experimental uncertainties. In all, however, the results for Pd, like those for Pt, are in generally fair agreement with Eq. (7) and known diffusion properties.

By dividing out the q^2 factor, the data presented in Fig. 8 offer a sensitive insight into the surface diffusion process. The solid lines in Fig. 8(a) fitted to the experimental points by the above procedure are derived for Pt by fitting diffusion coefficients in the domain where surface diffusion is dominant:

$$\mathrm{D}_s = 5(\times 2^{\pm 1}) \times 10^{-4} \exp(-1.2 \pm 0.1\ \mathrm{eV}/k_B T)\ \mathrm{cm}^2/\mathrm{s}.$$

For Pd, the fitted line gives

$$\mathrm{D}_s = 3(\times 2.5^{\pm 1}) \times 10^{-3} \exp(-1.1_5 \pm 0.1_5\ \mathrm{eV}/k_B T)\ \mathrm{cm}^2/\mathrm{s}.$$

A broader if less sensitive perspective on the results is obtained by comparing measured τ_q with values predicted from chosen diffusion coefficients. A comparison of this type

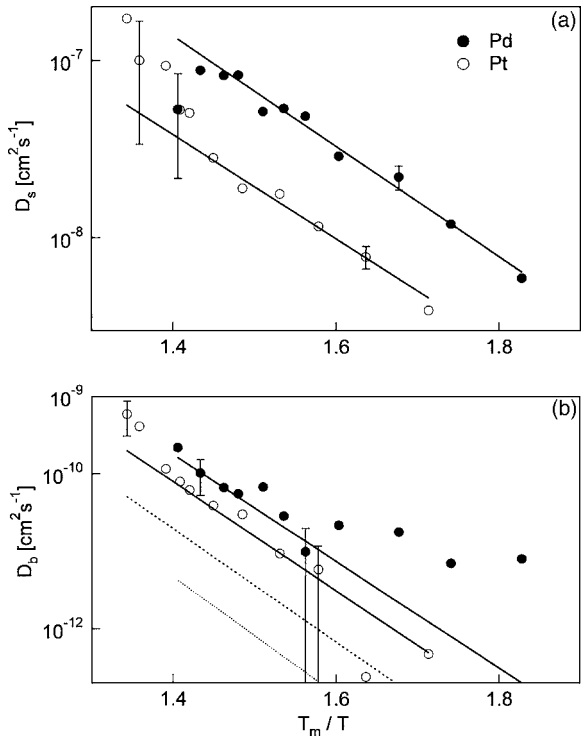

FIG. 8. Surface (a) and bulk (b) diffusion coefficients obtained by fits to Pt(111) and Pd(111) results in Fig. 7. For both surfaces, the scatter in (a) is large at high T and in (b) at low T, owing to increasing dominance of the competing process. The solid line through the Pt results in (b) represents published tracer results (Ref. 54) from this T range, while the dashed line is from tracer results extrapolated from high T (Refs. 55 and 56). The dotted line shows tracer results (Ref. 58) for Pd extrapolated from high T. The solid line through the Pd points is a least-squares fit for high temperatures.

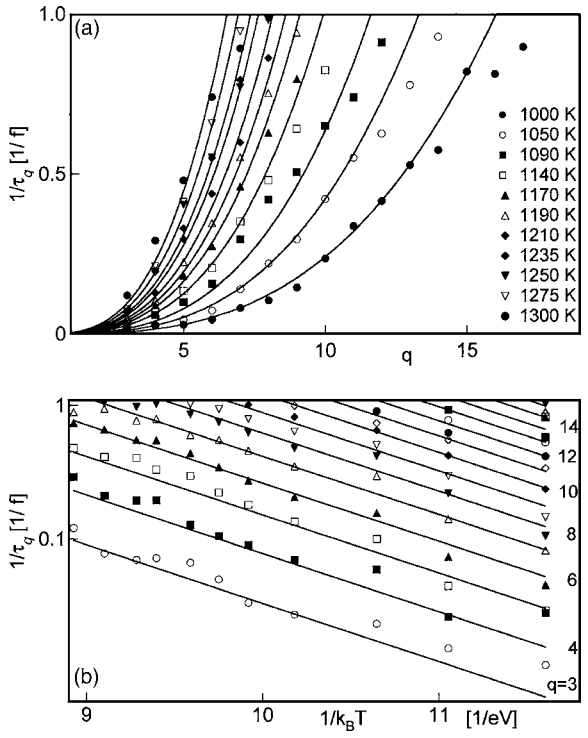

FIG. 9. Observed relaxation rates compared with predictions for Pd(111). In (a) the measured rates τ_q^{-1} are shown for various T as functions of q, and in (b), the T dependence is shown for selected values of q. The solid lines are predicted from Eq. (10) for $D_b = 0.2\exp(-2.75\ \mathrm{eV}/k_BT)\ \mathrm{cm}^2\ \mathrm{s}^{-1}$ and $D_s = 2.9\times 10^{-3}\exp(-1.1\ \mathrm{eV}/k_BT)\ \mathrm{cm}^2\ \mathrm{s}^{-1}$.

is shown for Pd in Fig. 9(a) as a function of q at fixed T and as a function of T at fixed q in Fig. 9(b). These graphs use data from the Hanning analysis and diffusion parameters:

$$D_b = 0.2\exp(-2.7_5\ \mathrm{eV}/k_BT)\ \mathrm{cm}^2/\mathrm{s},$$

$$D_s = 2.9\times 10^{-3}\exp(-1.2\ \mathrm{eV}/k_BT)\ \mathrm{cm}^2/\mathrm{s}.$$

The results are thus fairly insensitive to the type of analysis employed. Also, the diffusion parameters are close to those determined in Fig. 8. For Pt, a global fit to data obtained using the Hanning analysis yields

$$D_b = 0.55\exp(-2.7\ \mathrm{eV}/k_BT)\ \mathrm{cm}^2/\mathrm{s},$$

$$D_s = 5\times 10^{-4}\exp(-1.21\ \mathrm{eV}/k_BT)\ \mathrm{cm}^2/\mathrm{s}.$$

An earlier analysis with the triangle correction[7] gave noisier data and a similar D, and with

$$D_s = 2\times 10^{-4}\exp(-1.2_5\ \mathrm{eV}/k_BT)\ \mathrm{cm}^2/\mathrm{s}.$$

The differences are not large. From an analysis of surface scratches on Pt(111) smoothing during annealing, an activation energy of 1.12 eV for surface diffusion has been inferred.[59] This value, also, is in satisfactory agreement with the results reported above.

C. Multisteps

In an earlier brief note[10] the stiffnesses and kinetics reported for multisteps on Pt(111) were obtained by the triangle subtraction procedure, before the significance of correlations at $t\to\infty$ was recognized. The following account differs first in the use of the corrected analysis and, second, employs the Hanning procedure for kinetics. The resulting values $\tilde{\beta}$ and D_s are changed considerably in some cases.

Step stiffnesses obtained using the triangle subtraction, and now corrected for the correlations observed as $t\to\infty$ at 1500 K, are presented inset in Fig. 10 as solid circles. Results of the earlier approximate analysis[10] are indicated there by open circles. The revised values increase almost linearly with step number n. This is not the case in the absence of the $t\to\infty$ correction, as made apparent by Fig. 10. In the main panel of Fig. 10 the temperature dependences of the measured stiffnesses is reported. Only at 1500 K could values be determined for all n.

For the kinetics of multisteps, the present revisions employ the Hanning analysis of relaxation processes. The changed results nevertheless support global conclusions similar to those reported earlier using the "triangle" correction. We note here that the capillary derivation leading to

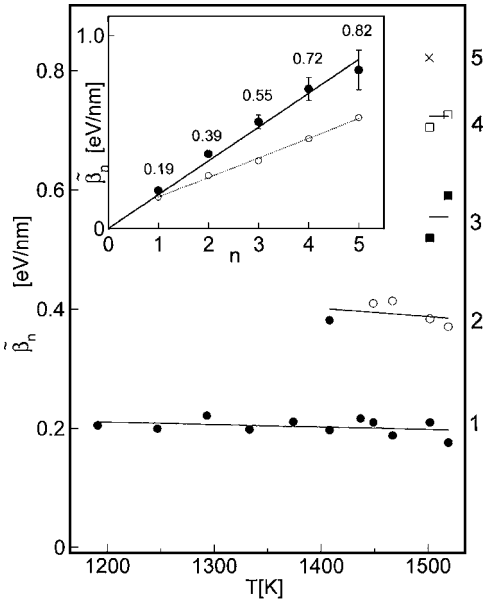

FIG. 10. Measured values of $\tilde{\beta}_n$ for multisteps on Pt (111) with $1 \leqslant n \leqslant 5$. For $n > 2$ results are available only above $T \sim 1400$ K. The grey circle at 1400 K for $n=2$ lies in the region of unstable steps. Inset compares the dependence of $\tilde{\beta}_n$ on n at 1500 K (solid circles) with solid line showing $\tilde{\beta}_n = n\tilde{\beta}_1$. Results of an earlier incomplete analysis (Ref. 10) are shown as open circles.

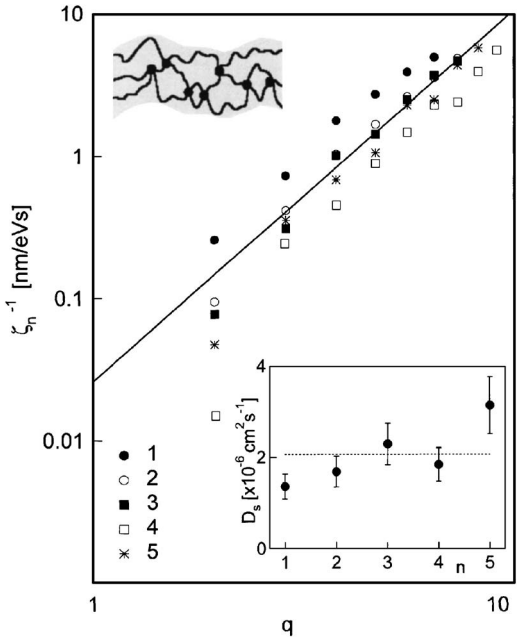

FIG. 11. Variation of $\zeta_n(q)^{-1}$ with q and n, determined from measurements of $\tilde{\beta}_n$ and τ_{nq}. The solid line indicates a $q^{2.5}$ dependence. The values are fairly independent of n, as predicted. Inset sketch at the top shows multistep modeled as a net with sparse contacts. Inset at the bottom shows an effective surface mass diffusion coefficient D_s as a function of n, here derived from the best-determined data ($3 < q < 7$) at 1500 K for Pt(111). This surface diffusion coefficient depends only weakly on step height (inset).

Eqs. (7) and (10) carries through for multisteps in all but one respect. That is, the multistep displacement must be written with A/n in place of the factor A employed for the single step, because n adatoms are required to move the multistep through the area per atom, A. Provided that the multistep structure causes no further complication in the kinetics, we may write for Eq. (10)

$$\frac{\pi k_B T n}{2\tau_{nq}\beta_n q^3 \Omega} = [D_s + (\pi/2qa)D_b] = D_{\text{eff}}, \tag{11}$$

in which τ_{nq} is the decay rate for the mode q of a multistep of height n. It follows that the quantity

$$\zeta_n(q) = \tilde{\beta}_n \tau_{nq}/n \tag{12}$$

should be independent of multistep height n and this is the basis upon which experiment is compared with prediction in what follows. [In a preliminary report the substitution $a = \Omega/A$ with Ω the atomic volume, was employed in Eq. (11) to identify, erroneously, A^2 in place of A there and, hence, n^2 in place of n in Eq. (12). We believe that ζ in the present Eq. (12) contains the correct scaling.]

In Fig. 11, ζ^{-1} is shown as a function of q for multisteps on Pt(111) for steps of height $n \leqslant 5$. To a fair approximation, the results for different multistep heights do fall close to the same line and so conform to the predicted scaling. Evidently the capillary modeling does provide a good first description of the multistep kinetics. A second perspective on this matter is presented inset in the main figure, where the effective surface diffusion coefficient, denoted by D_s, is derived for the best-determined data, which have $3 \leqslant q \leqslant 7$ at $T = 1500$ K, are shown as a function of step height n. Clearly, the kinetics of capillary fluctuations for steps of different height determine much the same terrace diffusion coefficient, independent of n and q. We conclude that the internal structure of the multisteps must lack major consequence for the kinetics of their equilibrium fluctuations, so that the behavior can be approximated by a capillary model, in agreement with an earlier assessment.[10] A model of multistep structure as a dilute network, shown inset in Fig. 11, is discussed below.

IV. DISCUSSION

The values of $\tilde{\beta}$ reported in Sec. III have generally similar features for Pt(111) and Pd(111). In several respects they also resemble earlier results obtained by step fluctuation spectroscopy for the metals Mo(011) (Ref. 8) and Au(111) (Ref. 9). In each case the step stiffness just above $T_m/2$ is ~ 250 meV/nm. The observed values of $\tilde{\beta}$ depend only weakly on temperature, apparently decreasing slightly with increasing T in several cases. In order of magnitude a free energy decrease of this size would identify a step entropy of $\sim k_B$/nm. One characteristic in which the several surfaces differ significantly is in the anisotropy of $\tilde{\beta}$. In the present work, Pd(111) and Pt(111) are much more isotropic than Au(111) and Mo(011) above $0.5T_m$. Too few surfaces have as yet been studied for systematic trends to be identified. Nevertheless, the differences among similar metals make it hard to see how these stiffnesses could find an explanation in

terms of macroscopic ideas such as elasticity. Furthermore, the stability with temperature change seems inconsistent with the possibility that the small step stiffnesses are a sum of large terms with opposite signs.

In contrast to the present observations, step roughening transitions, in which the step free energy becomes small or zero, have a striking effect on the appearance of a surface, as documented for Si(001) (Ref. 14) and S/Fe(011) (Ref. 11) studied by LEEM. What happens is that the step length increases without apparent bounds as the step profile undergoes progressively larger displacements of shorter periodicity. It has long been expected that metal surfaces would exhibit step roughening for entropic reasons connected with kink formation at elevated temperatures.[4,16] Our LEEM observations on clean metals at higher temperatures show no traces of any such roughening, only smooth fluctuations of average step profiles with average profiles determined by surface contours. Also, the magnitude of step entropy deduced above is consistent, for example, with modest fractional frequency changes for several atoms for each nanometer of step or else with some fractional change of step free energy between 0 K and T_m. Neither the step free energy nor its entropic portion can be calculated from first principles accurately at the present time, so a detailed explanation of the results is not possible.

The present results add to a discrepancy, by up to an order of magnitude, in the step stiffnesses reported for particular metal surfaces at high temperatures and at low temperatures.[16] In the case of Pt, for example, the low temperature value is reported as 3–4 eV/nm,[4,28] which agrees poorly with the value of 0.2 eV/nm determined here. Other than T, the main difference in the experiments lies in the equipment employed for observation, which is LEEM or REM at high temperatures and STM at low temperatures. It remains possible, of course, that major changes of stiffness occur at $T < T_m/2$, although no large changes have as yet been reported. Two merits of the LEEM results are that the q dependence affords multiple, mutually consistent determinations of $\tilde{\beta}$ at each T and that the elevated temperatures tend to reduce heterogeneous step trapping at defects or impurity islands.

Turning now to kinetics, we affirm that a systematic procedure is now in place to interpret fluctuation kinetics in terms of surface and bulk mass diffusion coefficients. Here once more the observed q dependence is an important asset that permits the clear separation of surface and bulk components. One caution is that the present analysis rests on a supposition that the two processes have additive effects, for which the validity remains a matter for future study.[17]

Within this framework, the step edges on Pt(111) and Pd(111) conform to a growing body of information that suggests that surface mass diffusion on close-packed metal surfaces may be notably systematic. Specifically, the diffusion coefficients are similar when shown homologously as a function of T/T_m. A strong trend of this type in *bulk* diffusion of metals has been known and documented[60,61] for decades. The analogous behavior has been suggested for metal surfaces also,[62,17] but the experimental information needed to assess the actual behavior has been lacking. The present results for surface mass diffusion are presented as functions of T_m/T in Fig. 12, together with results for Au(111) derived by similar means and reported elsewhere.[9] The corresponding bulk tracer results are shown also, for comparison. In the range of homologous temperatures shown, the three sets of surface data conform closely to a common trend from which they scatter by a factor typically less than 3. The line represents the average behavior suggested elsewhere:[63,17,27]

$$D_s = 5 \times 10^{-4} \exp - 6T_m/T \ \mathrm{cm}^2/\mathrm{s}.$$

The result for *surface* mass diffusion differs notably in both prefactor and activation energy from the documented average result $D_b = 0.3 \exp - 17T_m/T \ \mathrm{cm}^2/\mathrm{s}$ for *bulk* diffusion (see Fig. 12). This is hardly surprising given the large perturbation in the surface layer and the fact that the bulk process takes place via vacancy hopping whereas the surface diffusion is thought to occur by adatom motion. Various calculations support a view that the activation energy on close-packed surfaces is largely for defect formation, with perhaps 20%–30% for defect hopping.[63–65] Thus, an independent measurement of the hopping energy for Pt adatoms reports[66] 0.26 eV, which is to be compared with 1.2 eV for the sum of hopping and formation energies, as measured in the present research.

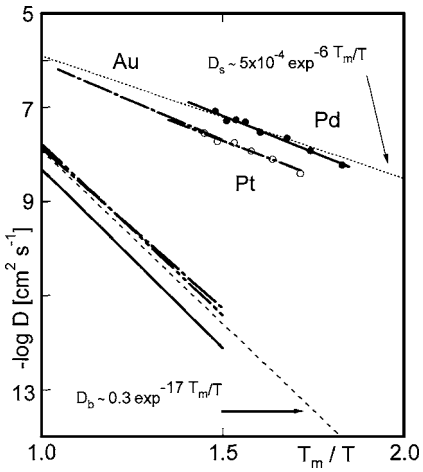

FIG. 12. Surface mass diffusion coefficients for the close packed surfaces Pt(111), Pd(111) (present data), and Au(111), shown as functions of T_m/T. The values of D_0 and the magnitudes of D are similar to an earlier suggestion (Ref. 17) $D_s \sim 5 \times 10^{-4}$ $\exp(-6T_m/T)$ indicated by the dashed line. Homologous behavior is known also for bulk diffusion D_b, shown for the same three metals.

Because both D_s and D_b are said to depend on T_m/T alone, it follows that their combination in Eq. (11) for step fluctuations takes this form also; some degree of universality is therefore to be expected in step relaxation phenomena, as outlined in more detail elsewhere.[17] In the results of Sec. III B, the behaviors of Pt and Pd are not identical, but the crossover from the surface regime to fluctuations dominated by bulk diffusion takes place at similar values of $T/T_m \sim 0.66$ as anticipated from the model and with similar absolute diffusion rates for the two metals.[17] This is true also for Au,[9] although in that case the data are more scattered owing to more difficult experimental conditions. In all, the experi-

ment on these close packed surfaces must be said to conform well to the suggested average behaviors.

Finally, with regard to the properties of multisteps, the observations reported for Pt(111) in this paper constitute a significant fraction of the total information currently available about multisteps. Multisteps on this surface form readily above 1400 K and are accessible to fluctuation analysis. The properties finally identified herein differ markedly from an earlier preliminary analysis,[10] but lead to parallel conclusions, summarized here.

From the present analysis, multistep energies on Pt(111) increase almost linearly with height n for $n \leqslant 5$ (see Fig. 10). Because $\tilde{\beta}$ is fairly isotropic, even for single steps (see, e.g., Fig. 4), we may take the measured isotropic stiffnesses $\tilde{\beta}_n$ of multisteps as approximate measures of the multistep free energies β_n. These structures possess also contributions of free energy due to the observed fluctuation modes. A reasonable estimate[10] of the extra free energy per atom length ($\sim$0.2 nm) due to capillary modes for $\varepsilon < k_B T$ is

$$f \sim \frac{1}{2} k_B T \ln \varepsilon / k_B T,$$

with ε the energy to make a kink. At 1500 K, typically $\ln(\varepsilon/k_B T) \sim -1$. Then $f \sim -0.25$ eV/nm is negative and comparable in magnitude with β_1, so that the net free energy of single steps is small and possibly negative. If multisteps were to possess the same number of capillary modes as single steps and a possibly larger ε_2, their negative contribution is smaller, while the positive line energy is larger, making a much larger positive sum. It now becomes impossible from these two contributions to the free energy *alone*, given the observed increase of β_n with n, to explain how two single steps reacting to form a two-step can cause a reduction of free energy.[10] This is nevertheless required by the observed reactions forming multisteps at 1400 K. The problem becomes progressively more intractable with increasing n. In the present work, this interesting fact is made still less tractable because the correct multistep energies are further *increased* relative to the single-step energy.

A suggested[10] resolution of this difficulty remains consistent with the accurate line energies reported here. It is that multisteps have internal structure and internal modes, whose excitation further reduces their net free energies at elevated temperatures. Internal structure is indeed visible on quenched multisteps examined near atomic resolution.[24] We speculate that these internal degrees of freedom are available for excitation. A limiting model is that multisteps comprise a network of single steps with sparse interconnections, so that the free energy per unit length of the component single steps is largely preserved in the combined structure. A cartoon of this structure, inset in Fig. 11, resembles an earlier suggestion from modeling.[67] The observed reactions, in which the network adds or subtracts unit steps, then reflect small differences in the two free energies that evidently change in the sense of favoring multisteps as the temperature is raised. It appears that fractional free energy differences on so fine a scale fall beyond the present capabilities for theoretical prediction, since neither the structures of multisteps nor their net free energies have as yet been calculated with success. The experimental facts reported here nevertheless provide quite specific insight into these complex phenomena.

The kinetics of multisteps, reported in Sec. III, also bear on multistep structure in an interesting way. Since their fluctuations, as described by capillary theory with the observed stiffnesses, are consistent with a common effective diffusion coefficient (Fig. 11), the actual internal structures can have little or no effect on the efficiency with which thermal defects exchange with the multistep. It seems reasonable that multisteps modeled by a loose network of single steps, as proposed here, could behave in the observed manner.

ACKNOWLEDGMENT

This research and the Center for Microanalysis of Materials in which the LEEM is maintained were supported in part by the Department of Energy Division of Materials Sciences through Grant Nos. DEFG02-91ER45439 and DEFG02-02ER46011.

*Corresponding author. FAX: +1 217 244 2278. Electronic address: ondrejce@uiuc.edu

[1] R. Gomer, Rep. Prog. Phys. **53**, 917 (1990).
[2] D. A. Reed and G. Ehrlich, Surf. Sci. **102**, 588 (1981).
[3] G. L. Kellogg, Surf. Sci. Rep. **21**, 1 (1994); A. Golzhauser and G. Ehrlich, Phys. Rev. Lett. **77**, 1334 (1996).
[4] For a review of step fluctuations see H.-C. Jeong and E. D. Williams, Surf. Sci. Rep. **34**, 171 (1999).
[5] N. C. Bartelt, J. L. Goldberg, T. L. Einstein, E. D. Williams, J. C. Heyraud, and J. J. Metois, Phys. Rev. B **48**, 15453 (1993).
[6] N. C. Bartelt, R. M. Tromp, and E. D. Williams, Phys. Rev. Lett. **73**, 1656 (1994); N. C. Bartelt and R. M. Tromp, Phys. Rev. B **54**, 11731 (1996).
[7] M. Ondrejcek, W. Swiech, G. Yang, and C. P. Flynn, Philos. Mag. Lett. **84**, 69 (2004); **84**, 417 (2004).
[8] M. Ondrejcek, W. Swiech, C. S. Durfee, and C. P. Flynn, Surf. Sci. **541**, 31 (2003).
[9] M. Ondrejcek, M. Rajappan, W. Swiech, and C. P. Flynn, Surf. Sci. **574**, 111 (2005).
[10] C. P. Flynn, M. Ondrejcek, and W. Swiech, Chem. Phys. Lett. **378**, 161 (2003).
[11] M. Ondrejcek, M. Rajappan, W. Swiech, and C. P. Flynn, J. Phys.: Condens. Matter **17**, S1397 (2005).
[12] M. P. A. Fisher, D. S. Fisher, and J. D. Weeks, Phys. Rev. Lett. **48**, 368 (1982).
[13] P. Nozières, in *Solids Far From Equilibrium*, edited by C. Godrèche (Cambridge University Press, Cambridge, England, 1991), p. 1.
[14] N. C. Bartelt, T. L. Einstein, and E. D. Williams, Surf. Sci. **312**, 411 (1994).

[15] C. P. Flynn, Phys. Rev. B **66**, 155405 (2002).
[16] M. Giesen, Prog. Surf. Sci. **68**, 1 (2001) and references therein.
[17] C. P. Flynn, Phys. Rev. B **71**, 085422 (2005).
[18] M. Ondrejcek, W. Swiech, R. S. Appleton, and C. P. Flynn (unpublished).
[19] S. Song, M. Moon, and S. G. J. Mochrie, Surf. Sci. **334**, 153 (1995).
[20] S. Dey, S. Kiriukhin, J. West, and E. H. Conrad, Phys. Rev. Lett. **77**, 530 (1996).
[21] C. P. Flynn, W. Swiech, R. S. Appleton, and M. Ondrejcek, Phys. Rev. B **62**, 2096 (2000).
[22] T. P. Pearl and S. J. Sibener, Surf. Sci. **496**, L29 (2002).
[23] O. Pierre-Louis and C. Misbah, Phys. Rev. B **58**, 2259 (1998); **58**, 2276 (1998).
[24] K. Sudoh, T. Yoshinobu, H. Iwasaki, and E. D. Williams, Phys. Rev. Lett. **80**, 5152 (1998).
[25] A. Pimpinelli and J. Villain, *Physics of Crystal Growth* (Cambridge University Press, Cambridge, England, 1998).
[26] A. Zangwill, *Physics at Surfaces* (*Cambridge University Press*, Cambridge, England, 1998).
[27] M. Ondrejcek, W. Swiech, and C. P. Flynn, Surf. Sci. **566–568**, 160 (2004).
[28] M. Giesen, G. S. Icking-Konert, D. Stapel, and H. Ibach, Surf. Sci. **366**, 229 (1996).
[29] W. K. Burton, N. Cabrera, and F. C. Frank, Proc. R. Soc. London, Ser. A **243**, 299 (1951).
[30] D. L. Adams, H. B. Nielsen, and M. A. Van Hove, Phys. Rev. B **20**, 4789 (1979).
[31] H. Ohtani, M. A. Van Hove, and G. A. Somorjai, Surf. Sci. **187**, 372 (1987).
[32] H. Marten and G. M. Ehmsen, Surf. Sci. **151**, 570 (1985).
[33] A. Eyers, F. Schäfers, G. Schönhense, U. Heinzmann, H. P. Oepen, K. Hünlich, J. Kirschner, and G. Borstel, Phys. Rev. Lett. **52**, 1559 (1984).
[34] L. Ilver, A. Kovacs, J. Kanski, P. O. Nilsson, and E. Sobczak, Phys. Scr. **35**, 726 (1987).
[35] N. Dahlbäck, P. O. Nilsson, and M. Pessa, Phys. Rev. B **19**, 5961 (1979).
[36] A. R. Sandy, S. G. J. Mochrie, D. M. Zehner, G. Grübel, K. G. Huang, and D. Gibbs, Phys. Rev. Lett. **68**, 2192 (1992).
[37] G. Grübel, K. G. Huang, D. Gibbs, D. M. Zehner, A. R. Sandy, and S. G. J. Mochrie, Phys. Rev. B **48**, 18119 (1993).
[38] J. F. van der Veen, R. G. Smeek, R. M. Tromp, and F. W. Saris, Surf. Sci. **79**, 219 (1979).
[39] A. Davis, D. P. Jackson, J. B. Mitchell, P. R. Norton, and R. L. Tapping, Phys. Lett. **54A**, 239 (1975).
[40] J. P. Toennies, J. Vac. Sci. Technol. A **5**, 440 (1987).
[41] B. Poelsema, R. L. Palmer, G. Mechtersheimer, and G. Comsa, Surf. Sci. **117**, 60 (1982).
[42] M. Bott, M. Hohage, T. Michely, and G. Comsa, Phys. Rev. Lett. **70**, 1489 (1993).
[43] C. Teichert, M. Hohage, T. Michely, and G. Comsa, Phys. Rev. Lett. **72**, 1682 (1994).
[44] A. Steltenpohl and N. Memmel, Surf. Sci. **454–456**, 558 (2000).
[45] M. K. Rose, A. Borg, T. Mitsui, D. F. Ogletree, and M. Salmeron, J. Chem. Phys. **115**, 10927 (2001).
[46] B. Poelsema, J. B. Hannon, N. C. Bartelt, and G. Kellog, Appl. Phys. Lett. **84**, 2552 (2004).
[47] S. Ogawa, Y. Tanishiro, K. Takayanagi, and K. Yagi, J. Vac. Sci. Technol. A **5**, 1735 (1987).
[48] M. Kalff, G. Comsa, and T. Michely, Surf. Sci. **486**, 103 (2001).
[49] R. M. Tromp and M. Reuter, Ultramicroscopy **36**, 99 (1991).
[50] F. J. Harris, Proc. IEEE **66**, 51 (1978).
[51] G. Ehrlich and F. G. Hudda, J. Chem. Phys. **44**, 1039 (1966).
[52] R. L. Schwoebel, J. Appl. Phys. **40**, 614 (1966).
[53] N. L. Peterson, Solid State Phys. **22**, 409 (1968).
[54] B. Million and J. Kucera, Kovove Mater. **4**(XI), 300 (1973).
[55] G. Kidson and R. Ross, *Radioisotopes in Scientific Research* (UNESCO, Paris, 1957).
[56] E. Cattaneo, E. Germagnoli, and F. Grasso, Philos. Mag. **80**, 1373 (1962).
[57] T. E. Vulin and R. W. Balluffi, Phys. Status Solidi **25**, 163 (1968).
[58] N. L. Peterson, Phys. Rev. **136**, A568 (1964).
[59] J. M. Blakely and H. Mykura, Acta Metall. **10**, 565 (1962).
[60] C. P. Flynn, *Point Defects and Diffusion* (Oxford University Press, New York, 1972).
[61] H. Schultz and P. Ehrhart, in *Atomic Defects in Metals*, edited by H. Ullmaier, Landolt-Börnstein, New Series, Group III, Vol. 25 (Springer, Berlin, 1991), p. 115.
[62] C. P. Flynn, J. Phys. F: Met. Phys. **18**, L195 (1988).
[63] P. M. Agrawal, B. M. Rice, and D. L. Thompson, Surf. Sci. **515**, 21 (2002).
[64] S. V. Eremeev, A. G. Lipnitskii, A. I. Potekeev, and E. V. Chulkov, Phys. Low-Dimens. Semicond. Struct. **3–4**, 127 (1997).
[65] Y. N. Devyatko, S. V. Rogozhkin, and A. V. Fadeev, Phys. Rev. B **63**, 193401 (2001).
[66] K. Kyuno, A. Golzhauser, and G. Ehrlich, Surf. Sci. **397**, 191 (1998).
[67] S. V. Khare, T. L. Einstein, and N. C. Bartelt, Surf. Sci. **339**, 353 (1995).